

STUDIES ON RADIATION SHIELDING
OF ENERGY DOUBLER MAGNETS (1)

H. Edwards, S. Mori, and A. Van Ginneken

December 27, 1978

I Introduction

Several measurements have been made to understand quench problems of superconducting magnets due to beam energy deposition in magnet coils.¹ Some preliminary analysis of quench problems of Energy Doubler magnets due to beam losses at injection, during acceleration and at extraction have already appeared.^{2,3} In this report we discuss radiation problems due to beam losses during acceleration and extraction. We also discuss various proposed schemes to minimize such problems.

II. Limits of Energy Deposition

Figure 1 shows an estimate of the relation between limits of energy deposition in superconducting coils and magnet excitation current.² These limits appear consistent with measurements.¹ Table I summarizes the limits for extraction beam losses.

Table I. Limits of energy deposition at extraction energy.

Mode	Limits
Slow	4 mw.g^{-1}
Fast (1ms)	$1 \text{ mj.g}^{-1} \cdot \text{pulse}^{-1}$
Abort (20 μs)	$0.5 \text{ mj.g}^{-1} \cdot \text{pulse}^{-1}$

We assumed that $I/I_{\max} \approx 0.9$ for the following reasons. Firstly, the highest energy deposited inside the coils always appears near the horizontal median plane because of magnetic field effects on charged secondary particles and because of the curvature of the magnets. The magnetic field strength inside the coils around the horizontal median plane is about 10% lower than the maximum field which appears at the top and bottom corners of the coils. Secondly, it seems to be reasonable to operate the Energy Doubler at a slightly lower current level than the extreme quench level.

III. Extraction Beam Losses

Extraction beam losses are primarily caused by beam scattering and nuclear interactions in the electrostatic septum wires and Lambertson septum magnets.

(A) Radiation Due to Scattering From Electrostatic Septum Wires:

The program CASIM⁴₅ was modified to calculate energy deposited in Doubler magnets⁵. The wire septum and dipole magnet string have been modelled in all relevant geometric detail including the presence of electric and magnetic fields. However, in the present study a string of four quadrupole magnets to be placed upstream of the dipole string were omitted. A schematic drawing of the arrangement is shown in Figure 2. Figure 3 shows the energy deposition in the dipole string as a function of depth for a shallow (0.59 cm thick) radial region located near the inner radius of the coils for a 1000 GeV proton beam (0.2 cm high) uniformly distributed over the lateral dimension of the wire. Curves are drawn to guide the eye. The collimator upstream of the magnet string was omitted. Two distinct peaks are seen. The first peak is due to radiation

through the upstream magnet surface and can be suppressed by placing a collimator in front of the magnet. This is shown in Figure 4. An iron collimator with a hole radius of 2 cm and a length of 2m was placed as shown in Figure 2. The first peak was suppressed by a factor of roughly 100. The second peak is most prominent near $\phi = \pi$ and is mainly due to high energy photons from neutral pions produced in the forward direction. The collimator reduced the energy density at the second peak in general, but its maximum value (near $\phi = \pi$) was not significantly lowered. This large energy deposition of $3 \times 10^{-3} \text{ GeV.cm}^{-3} (\text{inc. proton})^{-1}$ therefore presents a more difficult problem. Table II gives the maximum numbers of protons that can be extracted under these conditions. The extraction inefficiency was assumed to be 2.5%, i.e. 2.5% of protons strike septum wires.

Table II. Numbers of protons that can be extracted for the electrostatic septum arrangement shown in Figure 2.

Mode	Number of Protons
Slow	2.7×10^{12} protons/sec
Fast (1ms)	0.7×10^{12} protons/pulse

Those limits are unacceptably low, particularly for fast spill. T. Collins proposed a modification of a long straight section to provide a large β region in the horizontal plane⁶, shown in Figure 5. If conventional magnets are used at the middle of the straight section, this will considerably reduce energy deposition in the Doubler magnets. Detailed calculations are in progress. In this arrangement good field tracking between superconducting and conventional magnets is required.

A bump as large as 4 mrad may not be needed to achieve a sufficient reduction of energy deposition density at the Doubler

magnets. Then, as shown in Figure 6, a simpler bump by conventional magnets only which does not require the same high degree of field tracking is more attractive. The direction of the bump can be outward or inward in the radial direction.

(B) Radiation Due to Scattering From Lambertson Magnets:

Protons which are scattered out of the electrostatic septum wires may strike the Lambertson magnet septum region and may cause radiation in downstream Doubler magnet coils. Figure 7 shows the schematic drawing of the arrangement used in the calculation. The energy density distribution in the Doubler magnet is shown in Figure 8. It was assumed that a 1000 GeV proton beam (0.2 cm high) was uniformly distributed over the central (narrowest) region of the septum, and struck the upstream surface of the septum perpendicularly. Nearly all incident protons underwent nuclear interactions in the septum. The large peaks at the upstream end can be suppressed by a collimator as in the electrostatic septum case. Unlike in the latter case the second peak corresponding to neutral pion production does not appear there because the Lambertson magnets have enough absorbing material at the septum region in the forward direction. The maximum energy density is about $4 \times 10^{-4} \text{ GeV.cm}^{-3}$ (inc. proton on Lambertson magnet).⁻¹ Table III gives the maximum numbers of protons that can be extracted through the Lambertson magnets. The interaction rate of protons at the Lambertson magnets was assumed to be 0.63% which is obtained if one quarter of protons which strike the electrostatic septum wires intersect the Lambertson magnets.

Table III. Numbers of protons that can be extracted through the Lambertson magnets.

Mode	Number of Protons
Slow	7.9×10^{13} protons/sec
Fast (1ms)	2.0×10^{13} protons/pulse

These limits are quite acceptable. No special arrangement seems to be required for the Lambertson magnet area. However, the assumption that the beam is uniformly distributed on the septum region (Figure 7) is perhaps questionable. Figure 9 shows the energy density distribution when the protons were incident uniformly distributed over the first 3.2 m on the side surface of the no-field region of the septum with an angle of $30 \mu\text{rad}$. The energy density is much larger than in Figure 8. Furthermore, a second peak appear around $\phi = \pi$ as in the electrostatic septum case. If a large fraction of the protons lost at the Lambertson magnet is typified by this mode, then the limits given in Table III must be substantially lowered.

The Lambertson magnet arrangement for the beam abort system has a lower limit of energy deposition because of the single-turn extraction. However, in principle it may have less problems since the extraction can be done more cleanly. Of the order of 6×10^{10} protons are allowed to hit the septum.

IV. Beam Losses During Acceleration

Figure 10 shows the schematic drawing of the case in which protons strike the vacuum chamber of the Doubler magnet on the inside edge. The proton energy is 1000 GeV. Figures 11 and 12 show energy density distributions in the Doubler magnet coils as functions of azimuthal angle and coil radius when protons interact with the vacuum chamber at $\phi = 0$ (at the accelerator inner

radius as indicated in Figure 10). For the vacuum chamber radius of 3.68 cm, the energy density distribution has a sharp peak near the proton interaction point $\phi = 0$ and reaches about 2 GeV cm^{-3} (interacting proton) $^{-1}$, which corresponds to about $4 \times 10^{-8} \text{ mj. g}^{-1}$ (interacting proton) $^{-1}$. This peak density is much smaller and has a gentler dependence when the vacuum chamber is placed at 3.18 cm inner radius. The second peak which appears at the downstream outer radius ($\phi = \pi$) is again due to neutral pions produced in the forward direction. The peak values are roughly the same for the both cases.

Figures 13 and 14 show energy density distributions when protons interact with the inside edge of the vacuum chamber at $\phi = \pi$ (at the outer accelerator radius). Essentially all the characteristics of the energy density distributions are identical to those distributions shown in Figures 11 and 12 with the ϕ angles reversed except for the second peaks corresponding to neutral pions. The latter cases do not have a neutral pion peak for geometrical reasons.

The first peak can be suppressed by long scrapers ($\geq 3\text{m}$), for example at medium straight sections. However, the second peak of about $1 \times 10^{-9} \text{ mj g}^{-1}$ (interacting proton) $^{-1}$ when protons interact with the vacuum chamber inside edge at the accelerator inner radius is difficult to reduce by a simple arrangement. If long straight sections are available for beam scraping, an arrangement of a beam scraper and absorbers with a beam dump system of conventional magnets seems to be a good solution, as shown in Figure 6. If no long straight section is available for beam scraping, T. Collins proposed a special beam scraper arrangement at medium straight sections, as shown in Figures 15 and 16. This arrangement requires special dipole magnets of a larger aperture and half the length of the normal Doubler dipole magnet. Detailed studies are in progress.

V. Conclusions

A special beam bump arrangement is required at the long straight section where the electrostatic septum is installed for extraction. The Lambertson magnet areas for both the normal extraction and the beam abort system may not require any special system other than simple beam collimators.

Beam scraper systems which localize beam losses and minimize radiation to the Doubler magnet coils during acceleration may have to be installed in medium straight sections. Further detailed studies are needed.

References

1. H. Edwards, C. Rode, and J. McCarthy, IEEE Trans. on Magnetics, Vol. 1, Mag 13, 1977, p 666, and B. Cox, P.O. Mazur, and A. Van Ginneken, "Sensitivity of an Energy Doubler Dipole to Beam Induced Quenches", TM-828A, 1978.
2. H. Edwards, "Beam Abort System", Internal Report, June 3, 1977.
3. T. Collins, "Radiation on Magnet Coils from the Wire Septum", Internal Report, 1978.
4. A. Van Ginneken, "CASIM, A Program to Simulate Hadronic Cascades in Bulk Matter", FN-272, January 1975.
5. A. Van Ginneken, "Distribution of Heat Due to Beam Loss in Energy Doubler/Saver Type Superconducting Magnets", TM-685, September 13, 1976.
6. T. Collins, "High-beta Straight Sections for the Doubler", UPC No. 14, November 14, 1978.
7. T. Collins, "Charged Particle Distributions Estimate", Internal Report, 1978.

Figure Captions

- Figure 1. Limits of energy deposition in Doubler superconducting magnet coils.
- Figure 2. Schematic drawing of the arrangement of the electrostatic wire septum for extraction at a long straight section. The second unit is tilted by $30 \mu\text{rad}$ away from the normal orbit so that wires of the second unit do not intersect protons. The ϕ angle is measured from the inner accelerator radius in the median plane.
- Figure 3. Energy density distributions in Doubler magnet coils due to scattering from the extraction electrostatic wire septum for a shallow radial region of 3.81 cm to 4.40 cm. The incident proton energy was 1000 GeV. No collimator was present.
- Figure 4. Energy density distributions in Doubler magnet coils due to scattering from the extraction electrostatic wire septum for a shallow radial region of 3.81 cm to 4.40 cm. The incident proton energy was 1000 GeV. An iron collimator of a hole radius of 2 cm and a length of 2 m was placed upstream of the Doubler magnets.
- Figure 5. Schematic drawing of a modified high- β long straight section by T. Collins. (See Reference 3.)
- Figure 6. Schematic drawing of a bump arrangement of conventional B-2 magnets at a long straight section.
- Figure 7. Schematic drawing of the Lambertson septum magnet arrangement for extraction.

Figure 8. Energy density distributions in Doubler magnet coils due to scattering from the extraction Lambertson septum magnets for a shallow radial region of 3.81 cm to 4.40 cm. It was assumed that 1000 GeV protons were distributed uniformly over the central region of the septum and struck perpendicularly the upstream surface of the septum. No collimator was present.

Figure 10. Energy density distributions in Doubler magnet coils due to scattering from the extraction Lambertson septum magnets for a shallow radial region of 3.81 cm to 4.40 cm. It was assumed that 1000 GeV protons struck the side surface of the septum from the normal beam orbit side with an angle of 30 μ rad, uniformly distributed over the first 3.2 m of the septum. No collimator was present.

Figure 11. Schematic drawing of the case in which 1000 GeV protons strike the vacuum chamber of a Doubler magnet. The proton beam was assumed to have a distribution of a δ -function in the vertical direction and interact the inside edge of the vacuum chamber in the median plane. The vacuum chamber radius is from 3.18 to 3.31 cm and 3.68 to 3.81 cm. The ϕ angle is measured from the inner accelerator radius in the median plane.

Figure 12. Energy density distributions in Doubler magnet coils due to beam losses on the vacuum chamber. The proton beam of 1000 GeV struck the inside edge of the vacuum chamber at the inner accelerator

radius ($\phi = 0$). The vacuum chamber radius was from 3.68 cm to 3.81 cm. The inner radius of the superconducting coils was 3.81 cm.

Figure 13. Energy density distributions in Doubler magnet coils due to beam losses on the vacuum chamber. The proton beam of 1000 GeV struck the inside edge of the vacuum chamber at the inner accelerator radius ($\phi = 0$). The vacuum chamber radius was from 3.18 to 3.31 cm. The inner radius of the superconducting coils was 3.81 cm.

Figure 14. Energy density distributions in Doubler magnet coils due to beam losses on the vacuum chamber. The proton beam of 1000 GeV struck the inside edge of the vacuum chamber at the outer accelerator radius ($\phi = \pi$). The vacuum chamber radius was from 3.68 cm to 3.81 cm. The inner radius of superconducting coils was 3.81 cm.

Figure 15. Energy density distributions in Doubler magnet coils due to beam losses on the vacuum chamber. The proton beam struck the inside edge of the vacuum chamber at the outer accelerator radius ($\phi = \pi$). The vacuum chamber radius was from 3.18 cm to 3.31 cm. The inner radius of superconducting coils was 3.81 cm.

Figure 15. Schematic drawing of a modified medium straight section with two half-bending magnets and beam scraper arrangement proposed by T. Collins (See Reference 3.).

Figure 16. Trajectories of neutral particles scattered from edges of the beam scraper in a Collins' modified medium straight section (See Reference 3.).

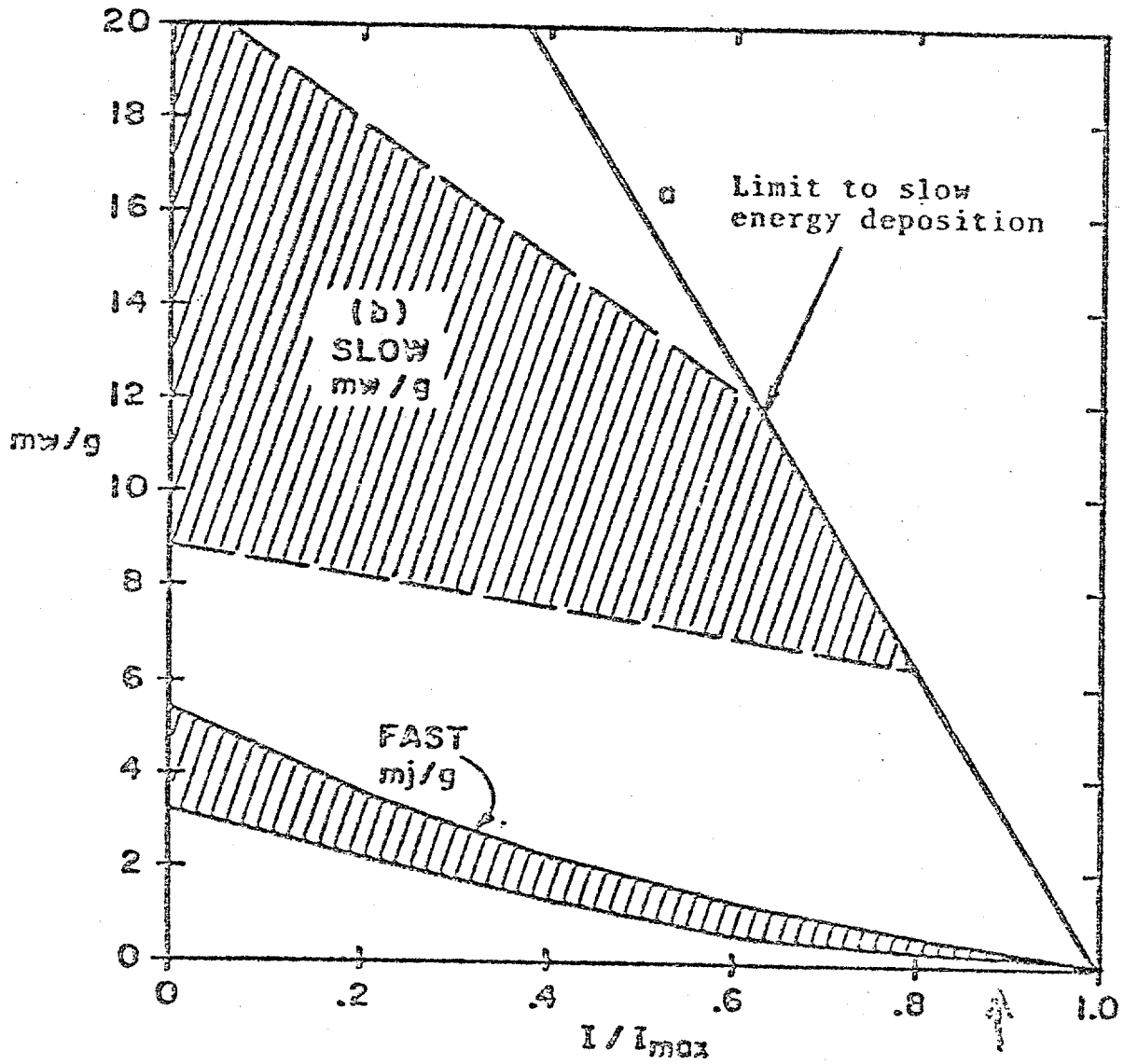
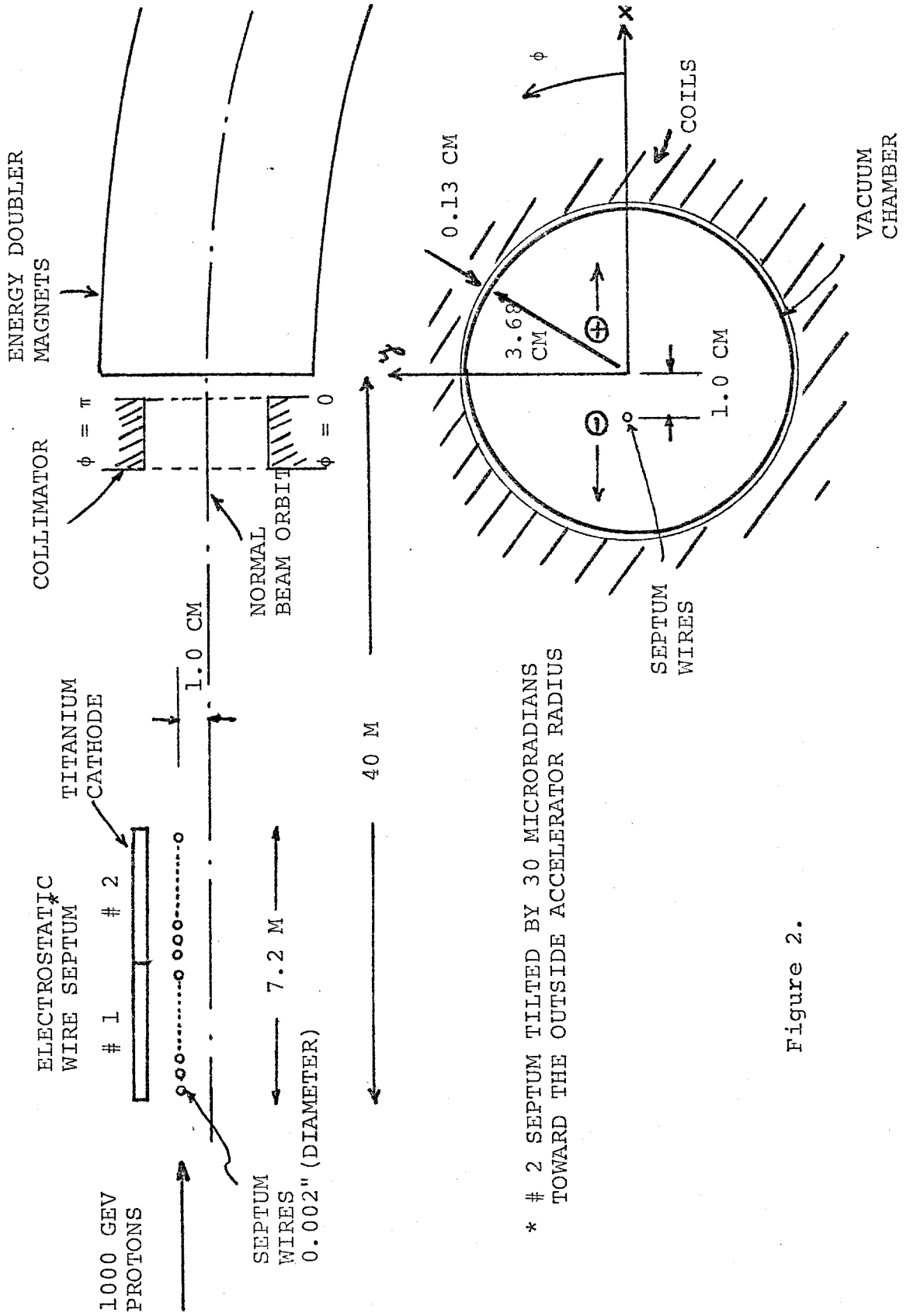


Figure 1. LIMITS OF ENERGY DEPOSITION IN DOUBLER SUPERCONDUCTING MAGNETS.

ELECTROSTATIC WIRE SEPTUM



* # 2 SEPTUM TILTED BY 30 MICRORADIANS TOWARD THE OUTSIDE ACCELERATOR RADIUS

Figure 2.

ENERGY DEPOSITION IN DOUBLER MAGNETS
DUE TO SCATTERING FROM
ES WIRE SEPTUM

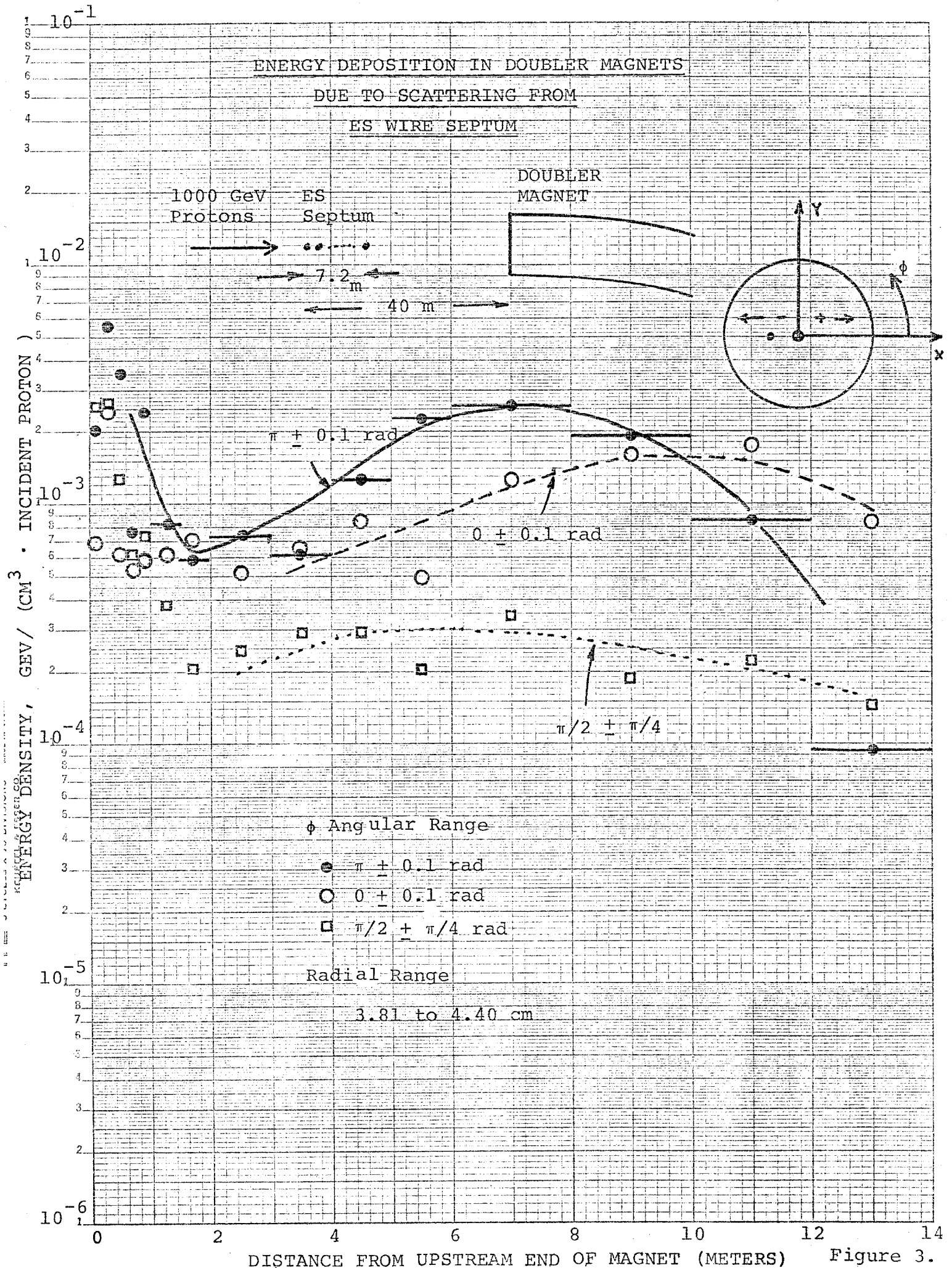


Figure 3.

ENERGY DEPOSITION IN DOUBLER MAGNETS
DUE TO SCATTERING FROM
ES WIRE SEPTUM

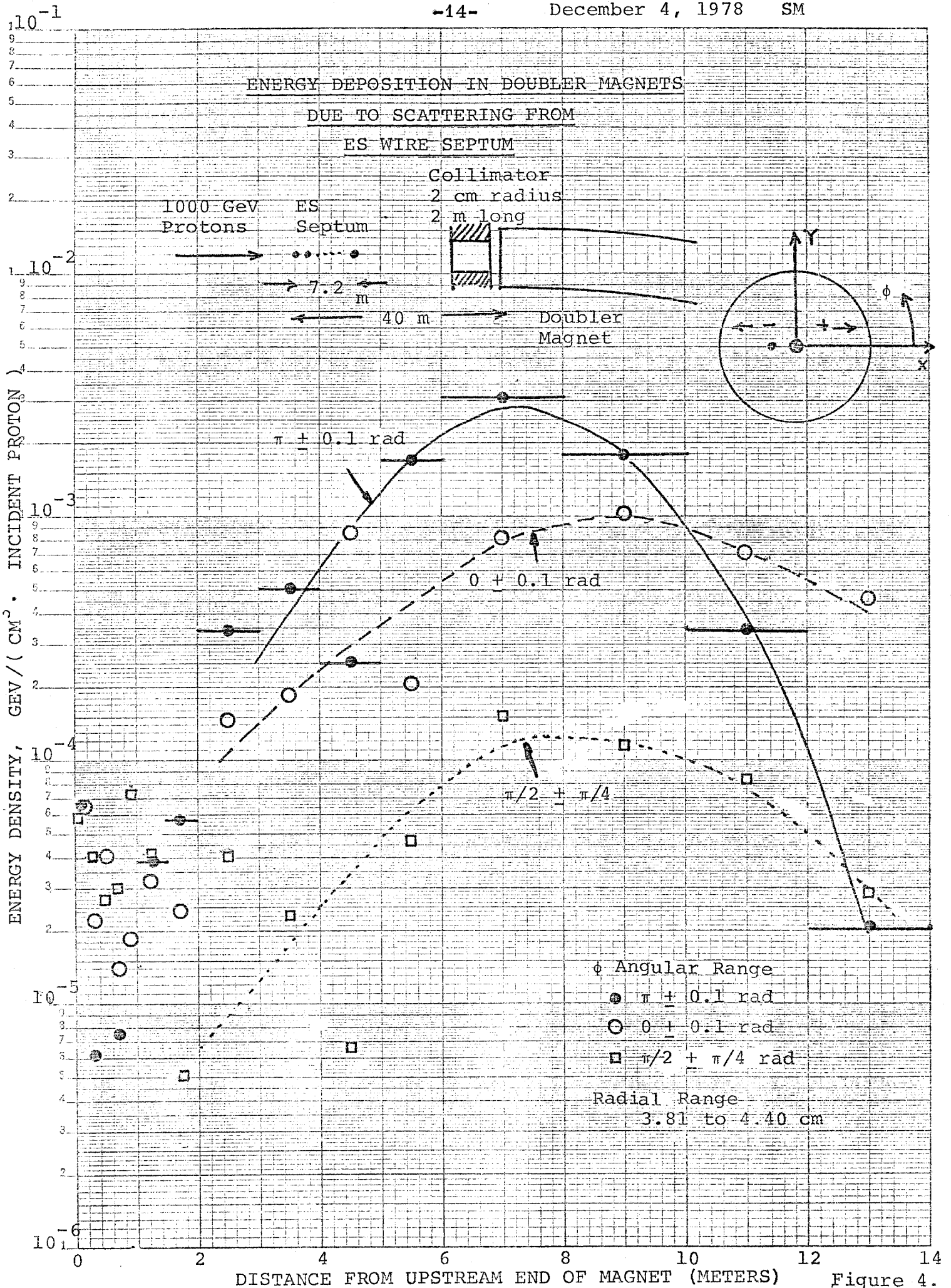


Figure 4.

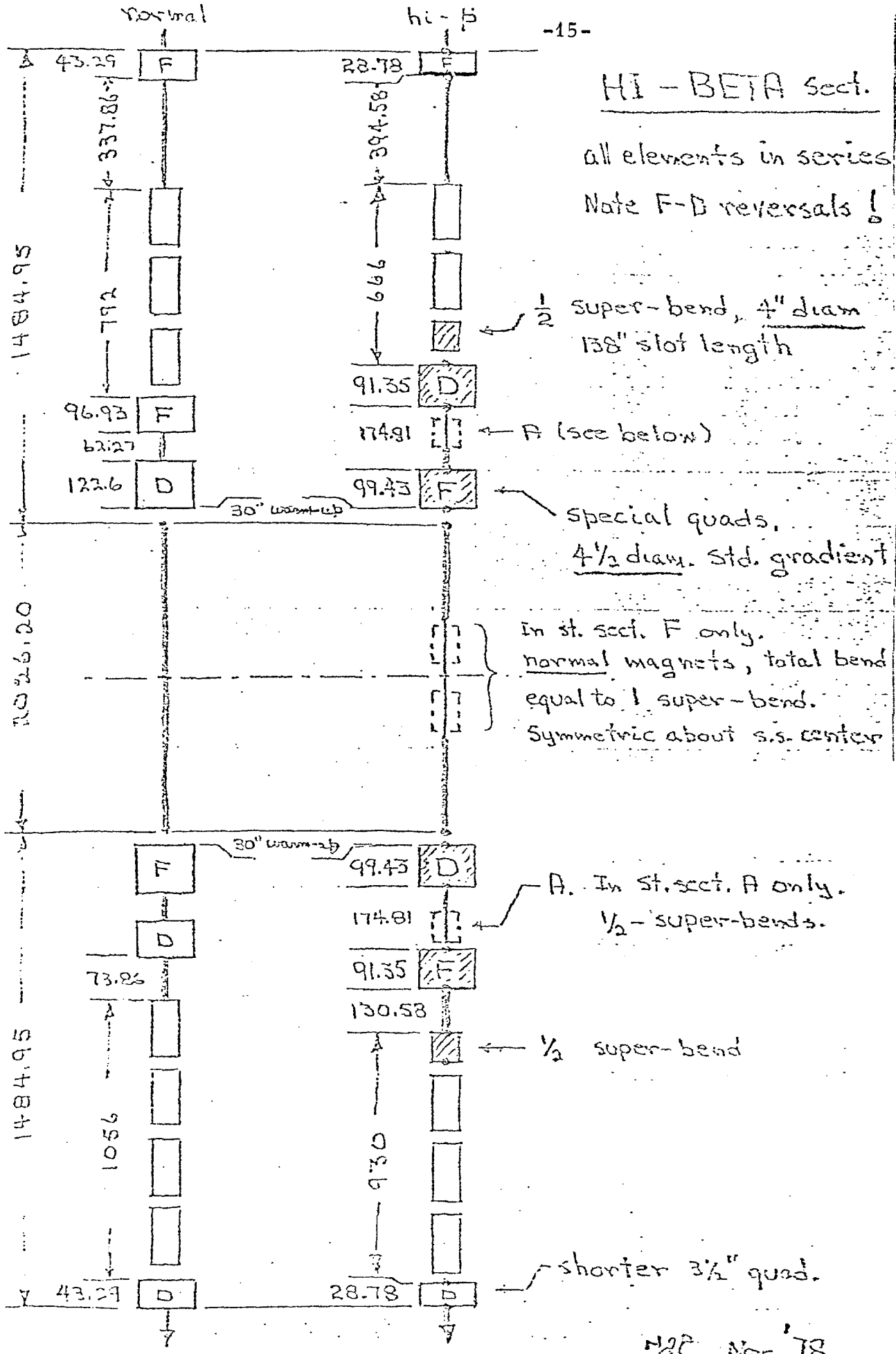
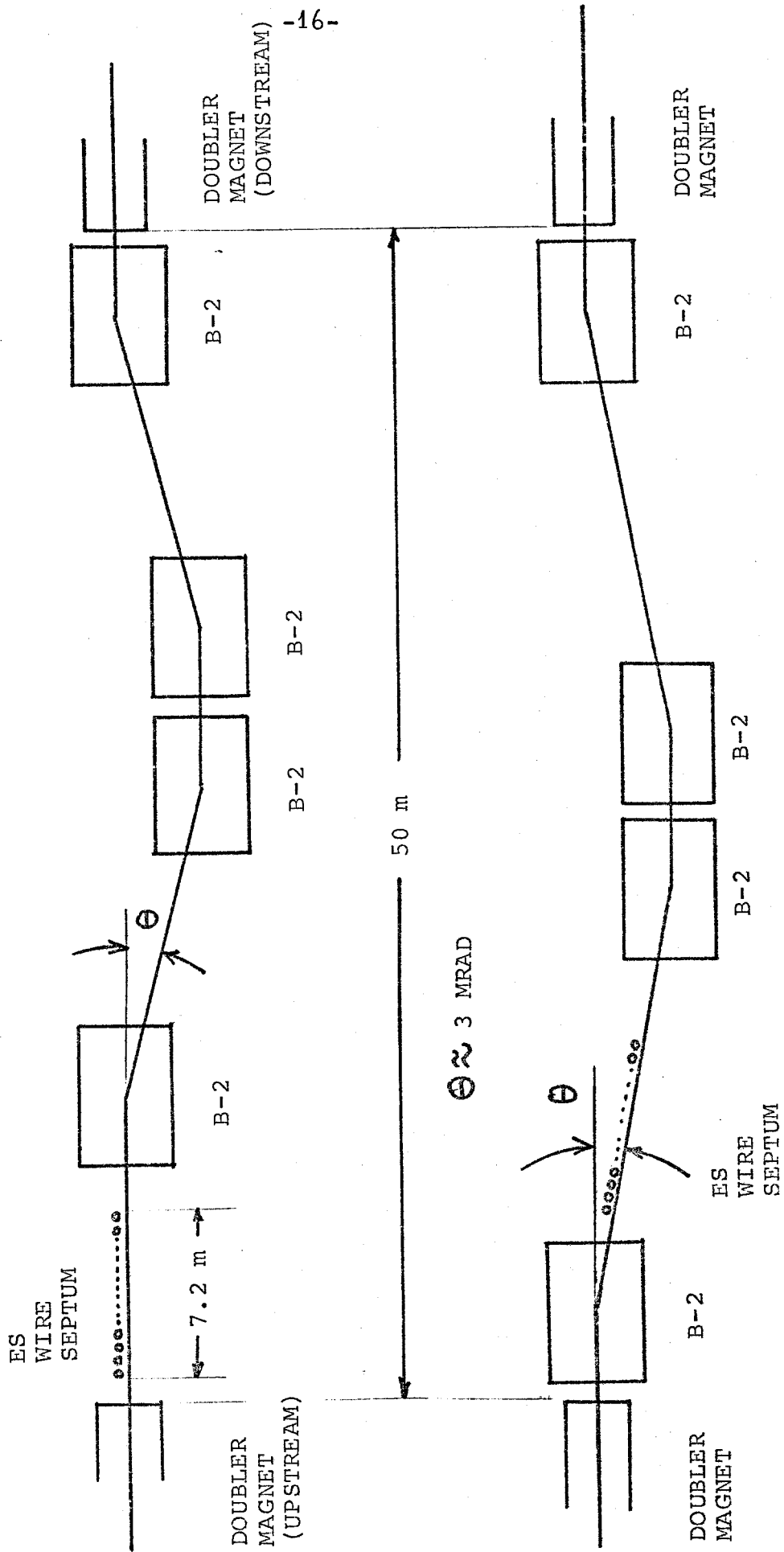


Figure 5.

2/8 Nov. '78

SIMPLE BUMP BY CONVENTIONAL MAGNETS (B-2)

AT F0 LONG STRAIGHT SECTION*



* COLLIMATORS PLACED INSIDE AND/OR IN FRONT OF B-2 MAGNETS DOWNSTREAM OF THE ES WIRE SEPTUM.

Figure 6.

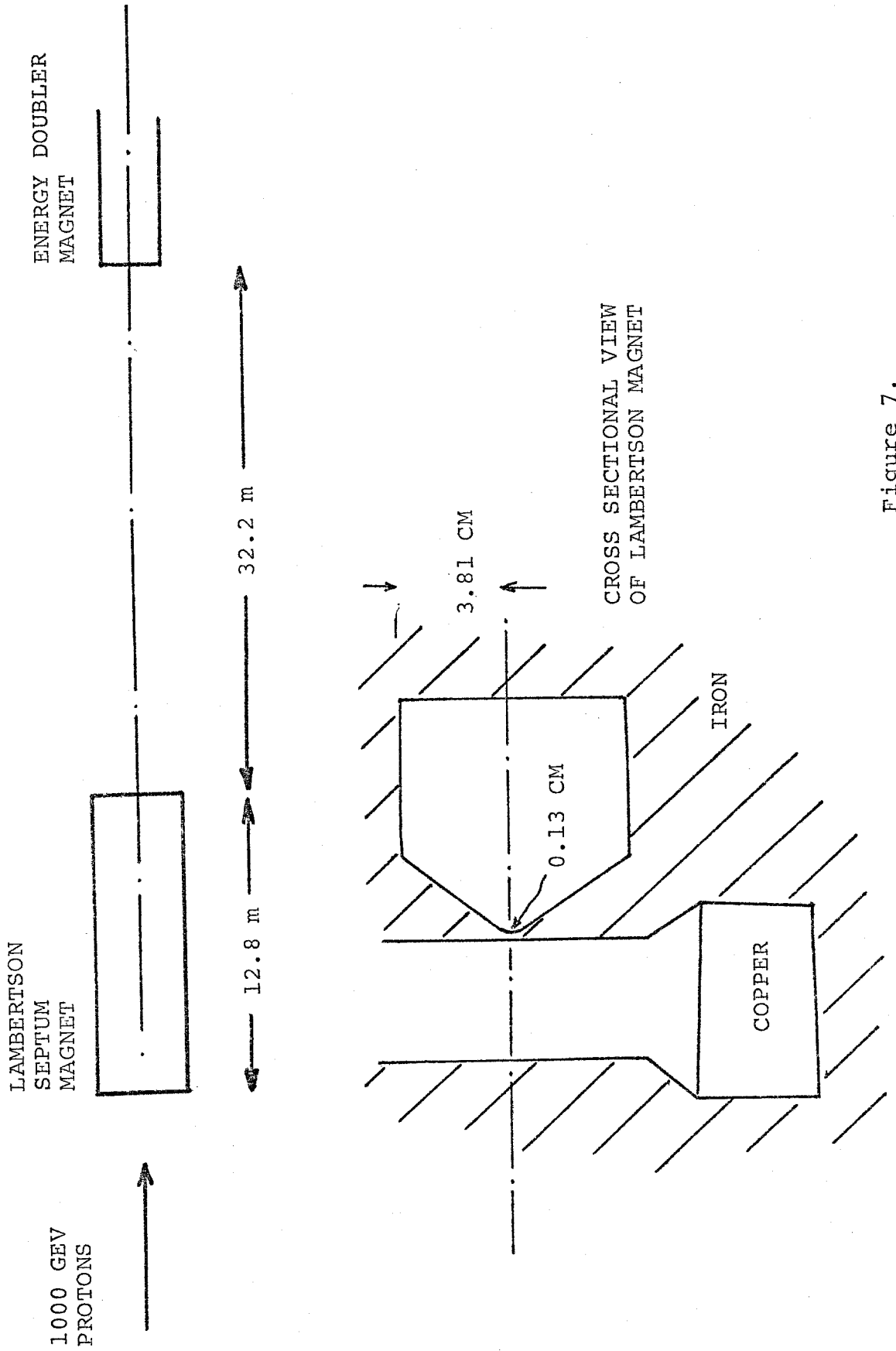


Figure 7.

ENERGY DEPOSITION IN DOUBLER MAGNETS
DUE TO SCATTERING FROM
LAMBERTSON SEPTUM MAGNET

PROTON ENERGY = 1000 GEV
NO COLLIMATOR USED
PROTONS INCIDENT ON SEPTUM
UNIFORMLY AND PARALLEL

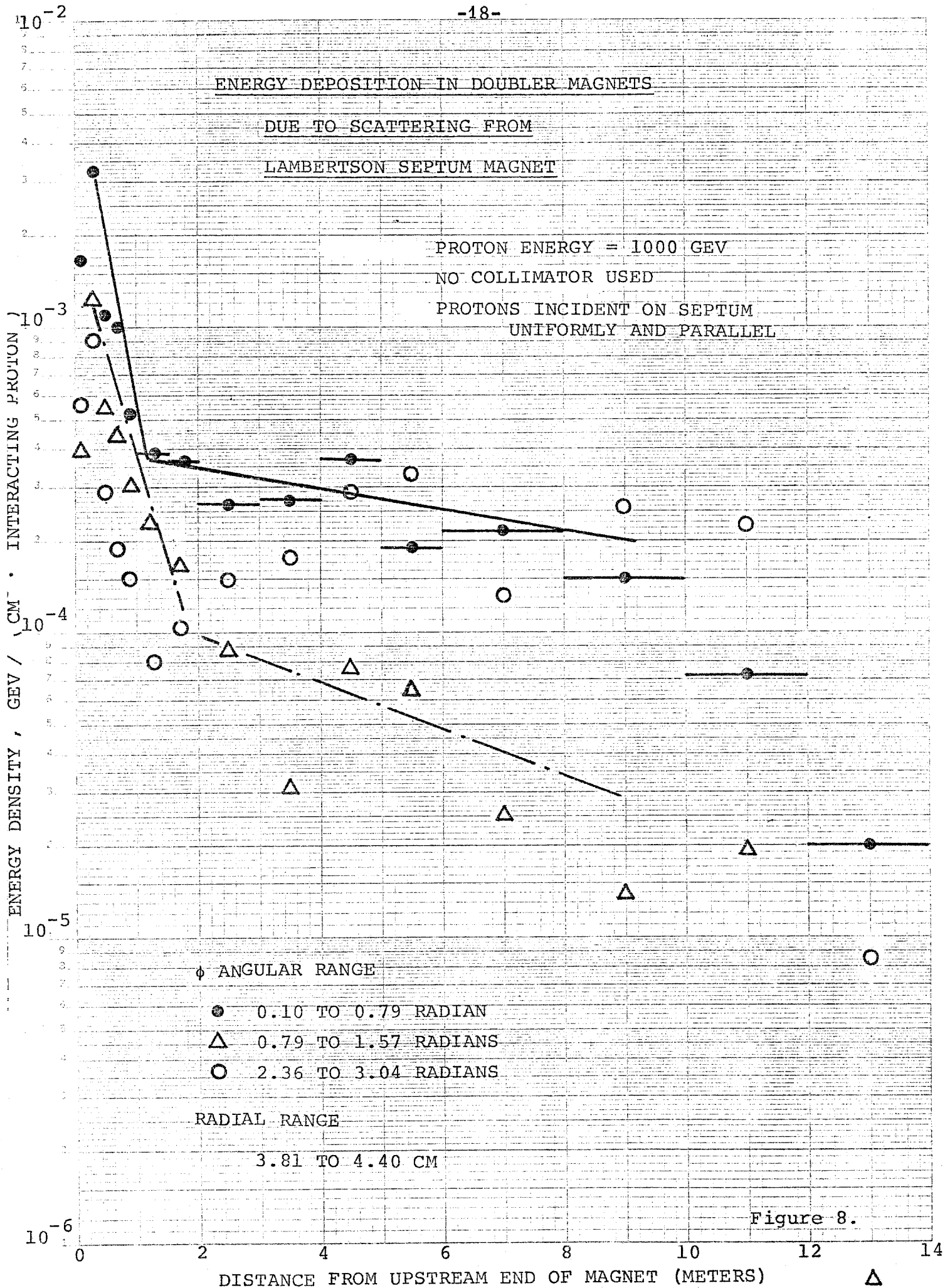


Figure 8.

ENERGY DEPOSITION IN DOUBLER MAGNETS

DUE TO SCATTERING FROM

LAMBERTSON SEPTUM MAGNET

PROTON ENERGY = 1000 GEV

NO COLLIMATOR USED

PROTONS INCIDENT FROM THE SIDE SURFACE
OF NO FIELD REGION WITH AN ANGLE
OF 30 MICRORADIAN

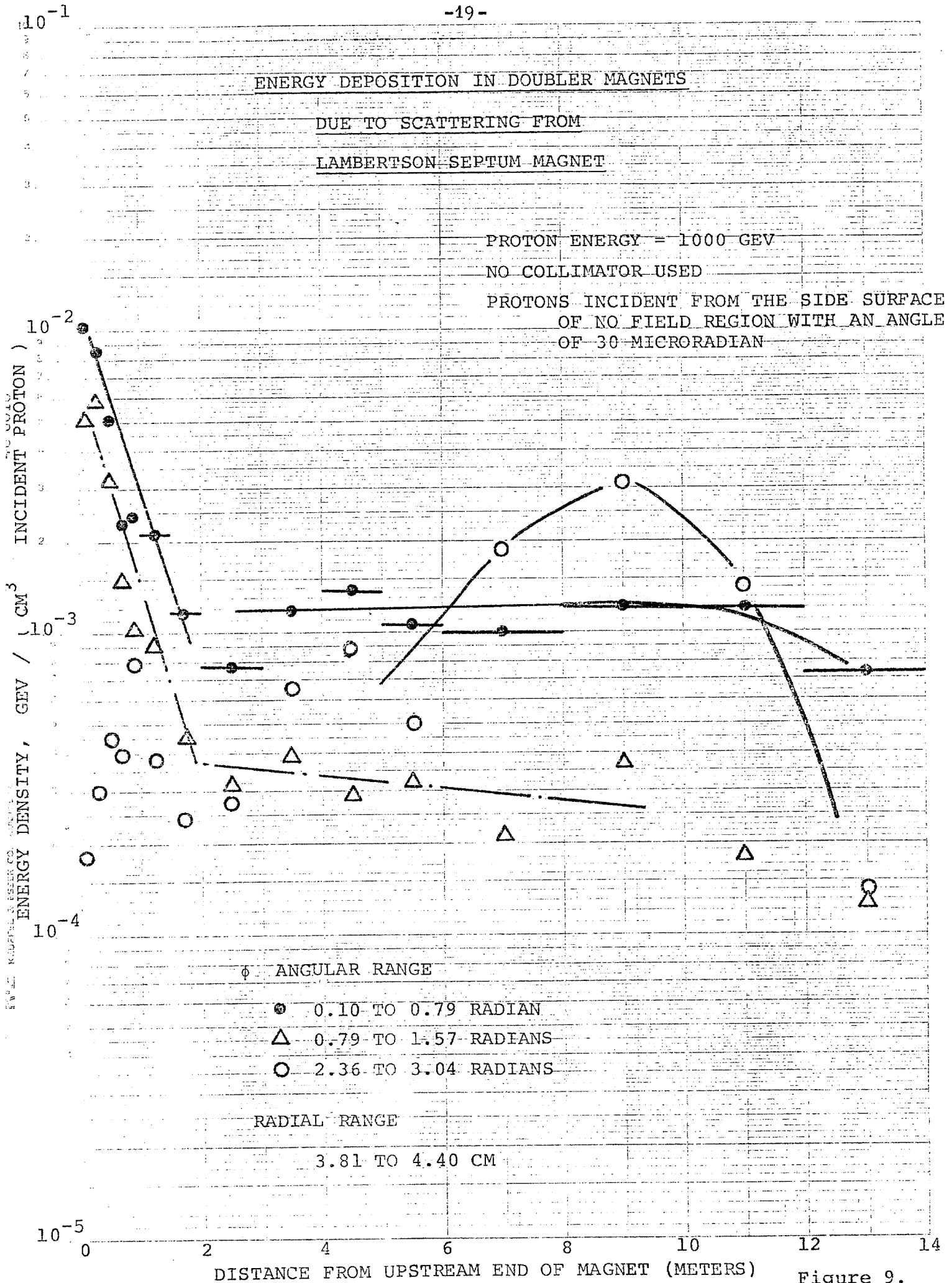
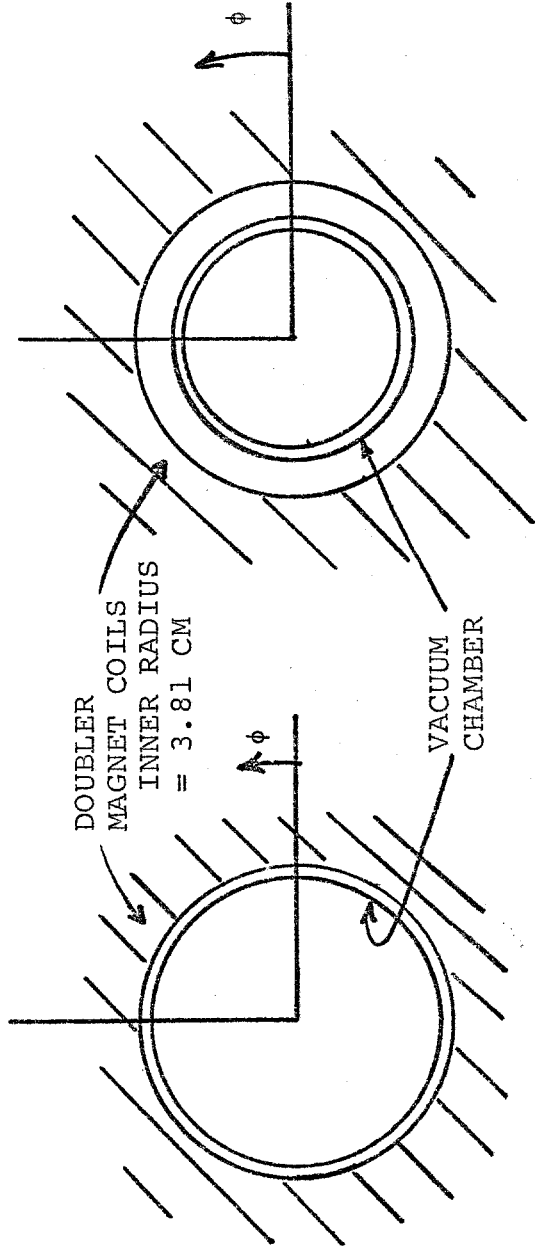
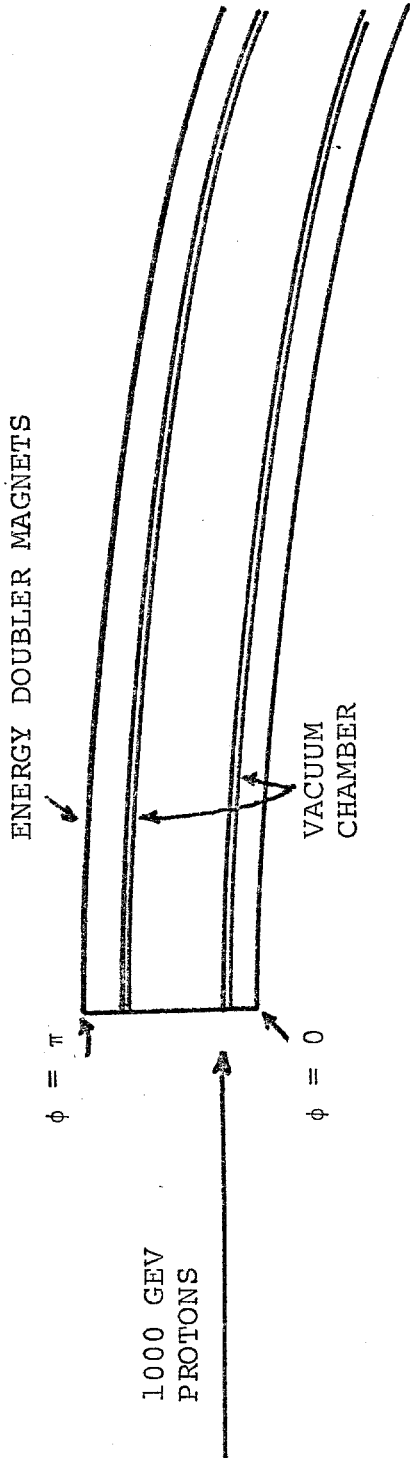


Figure 9.

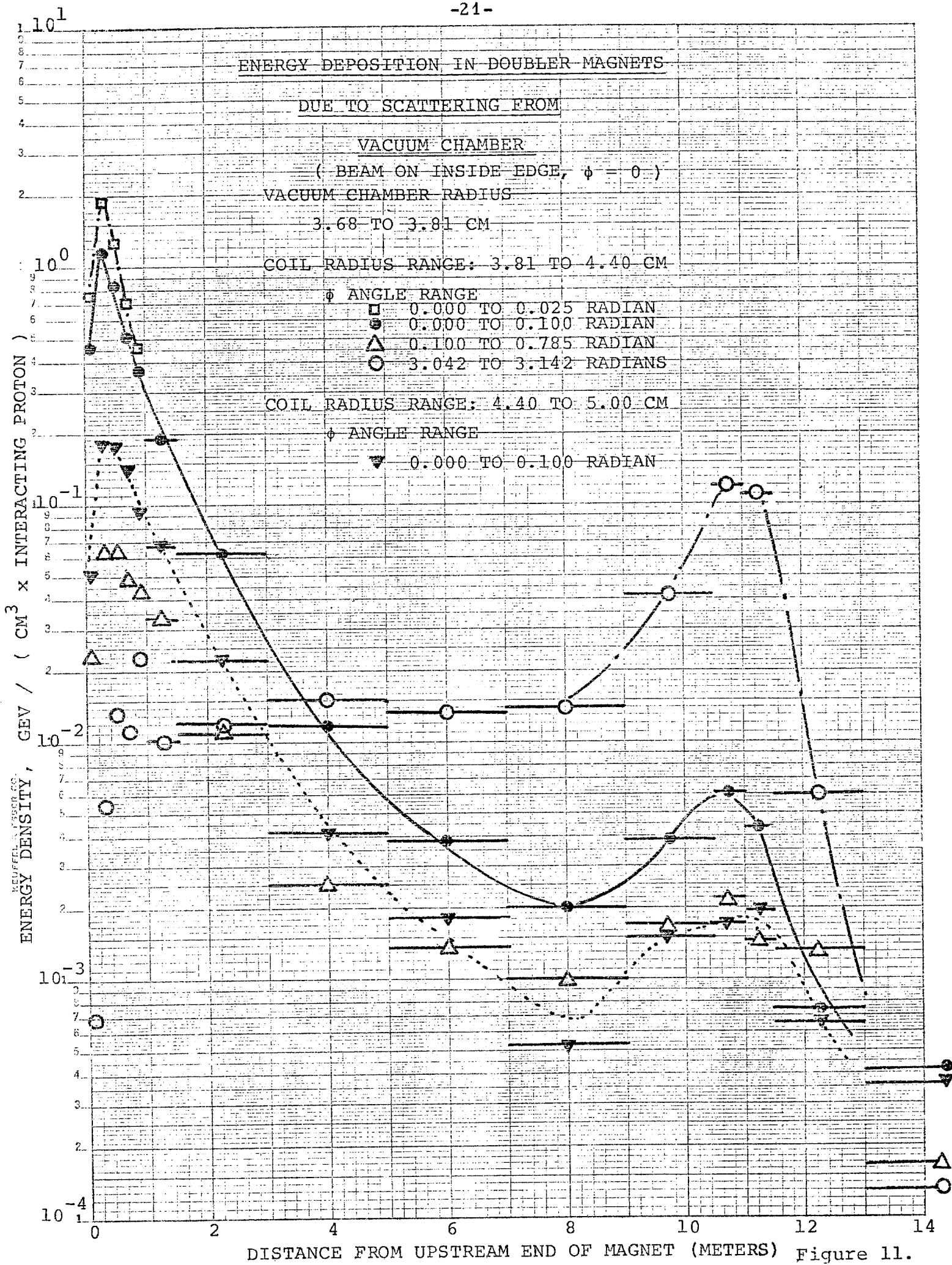
STRAIGHT HIT ON VACUUM CHAMBER BY 1000 GEV PROTONS



(I) VACUUM CHAMBER
INNER RADIUS = 3.68 CM
OUTER RADIUS = 3.81 CM

(II) VACUUM CHAMBER
INNER RADIUS = 3.18 CM
OUTER RADIUS = 3.31 CM

Figure 10.



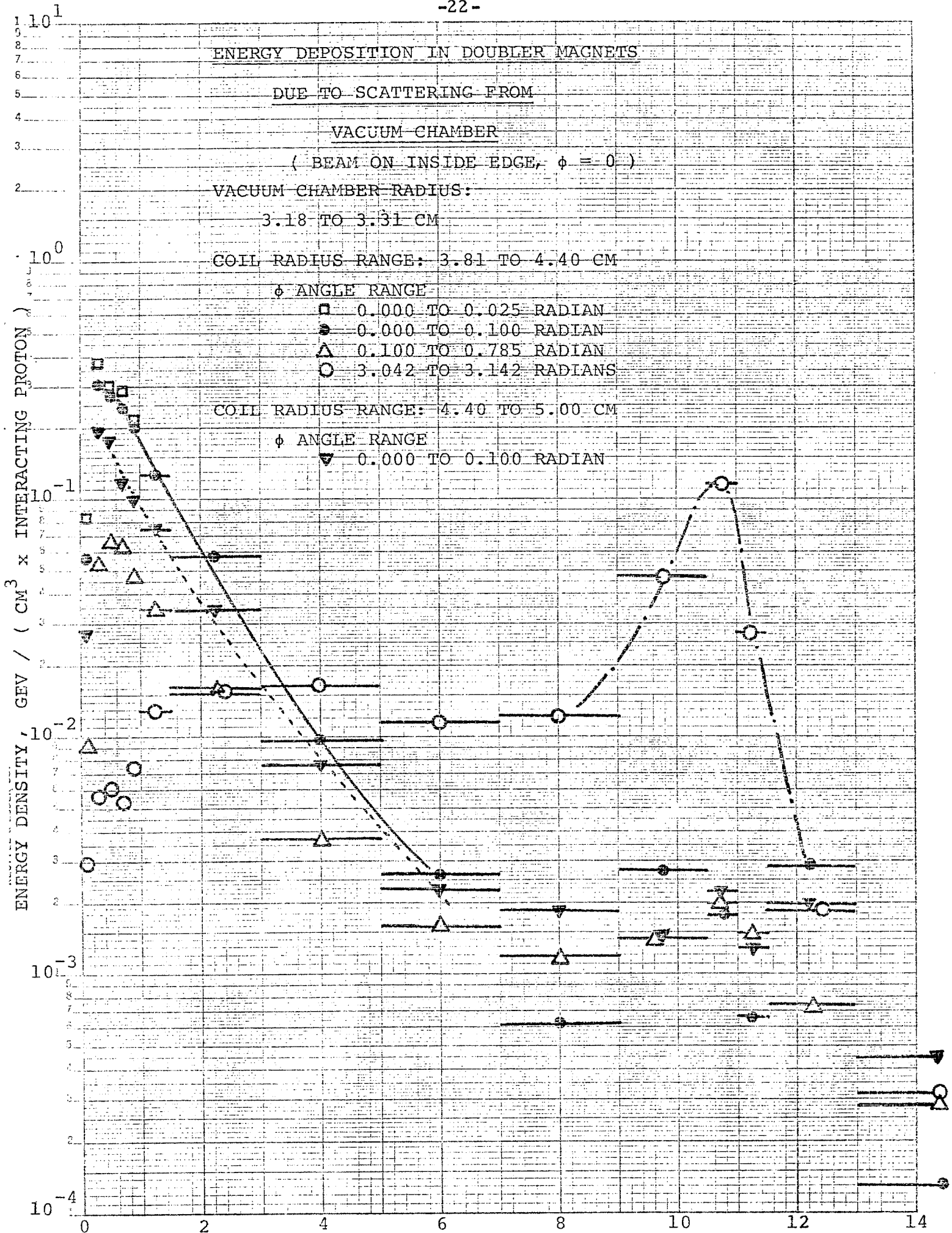


Figure 12.

ENERGY DEPOSITION IN DOUBLER MAGNETS

DUE TO SCATTERING FROM

VACUUM CHAMBER

(BEAM ON INSIDE EDGE, $\phi = \pi$)

VACUUM CHAMBER RADIUS: 3.68 TO 3.81 CM

COIL RADIUS RANGE: 3.81 TO 4.40 CM

ϕ ANGLE RANGE

● 0.000 TO 0.100 RADIAN

△ 2.350 TO 3.042 RADIANS

○ 3.042 TO 3.142 RADIANS

□ 3.117 TO 3.142 RADIANS

COIL RADIUS RANGE: 4.40 TO 5.00 CM

ϕ ANGLE RANGE

▼ 3.042 TO 3.142 RADIANS

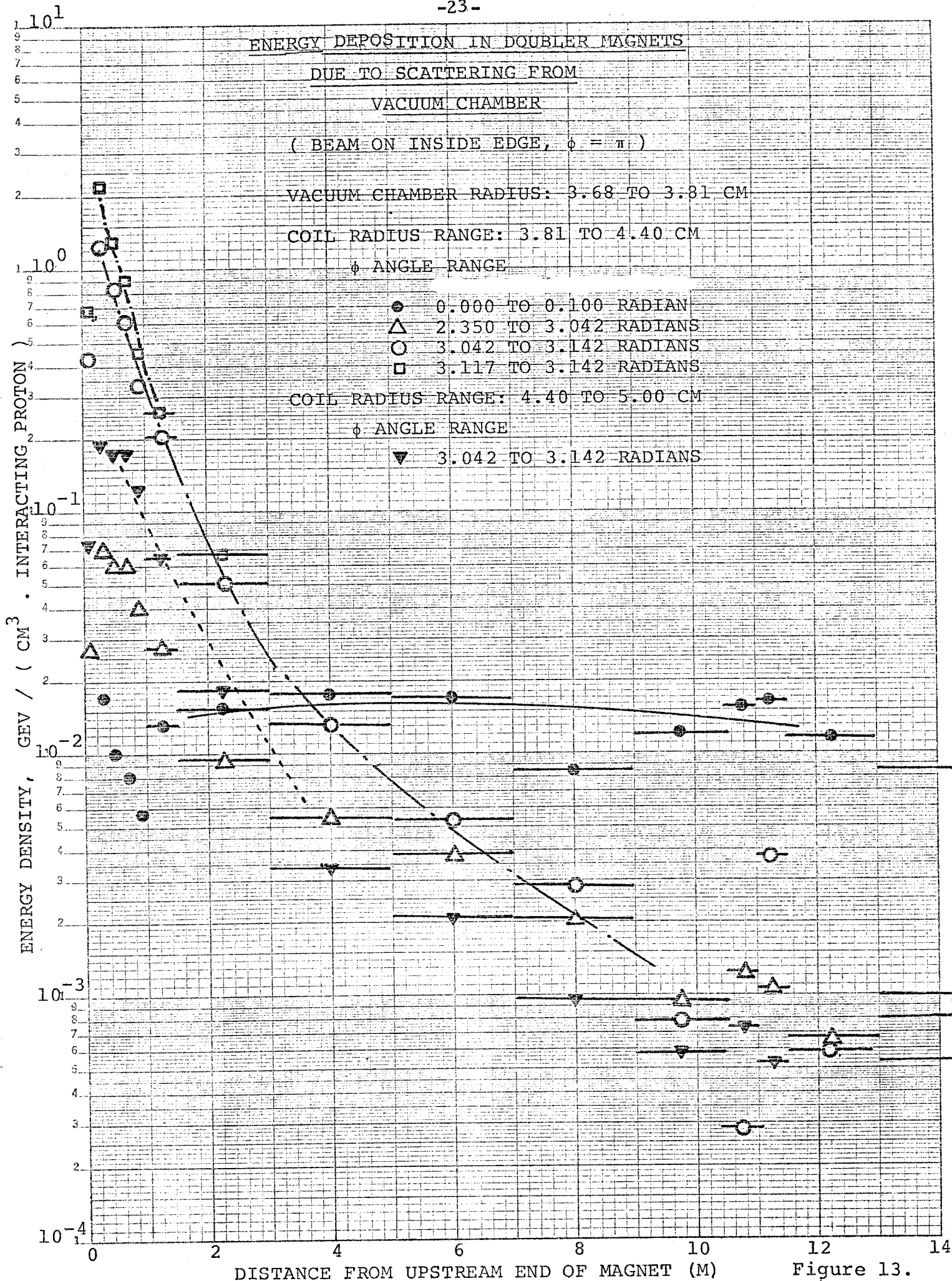


Figure 13.

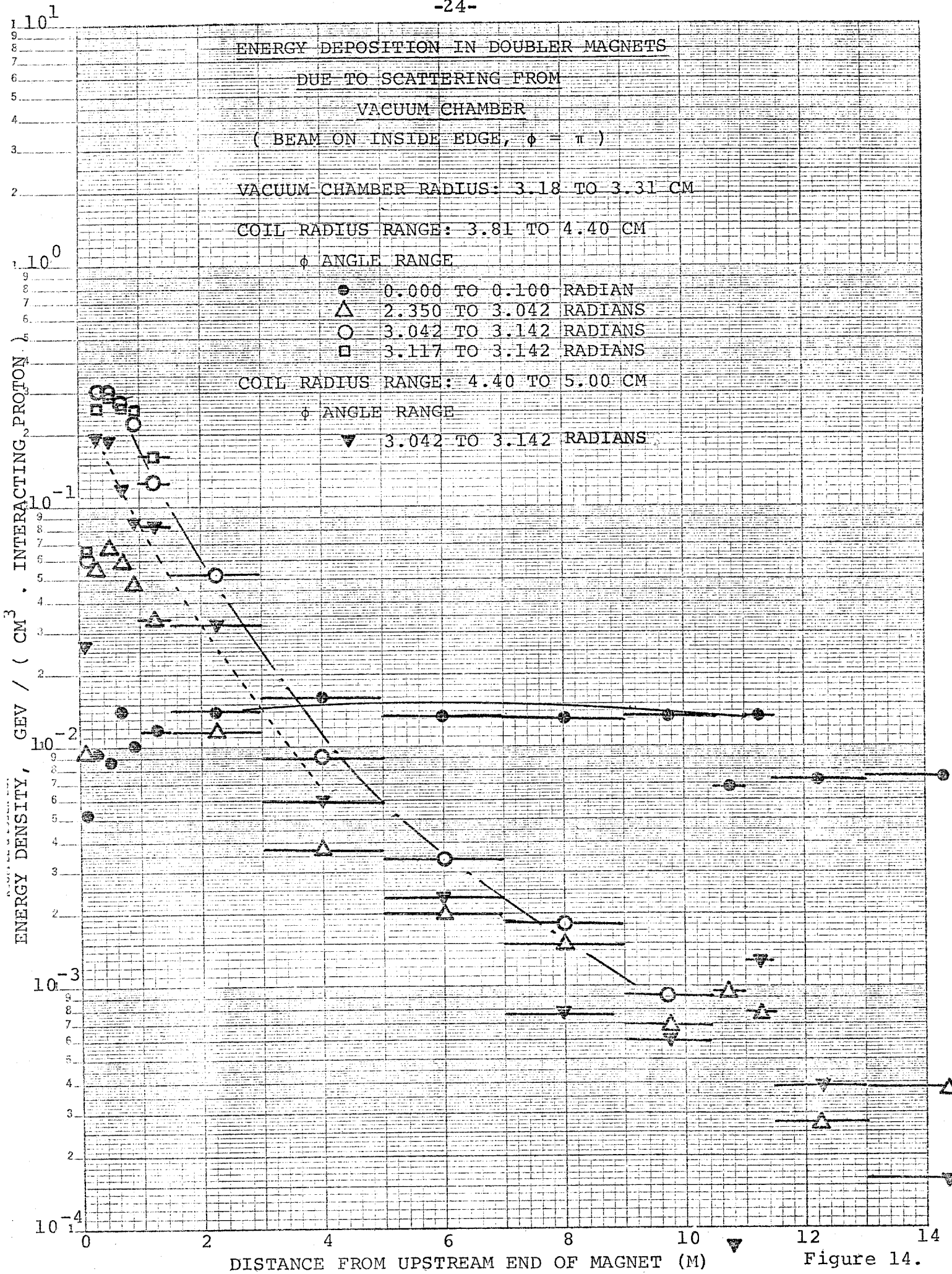
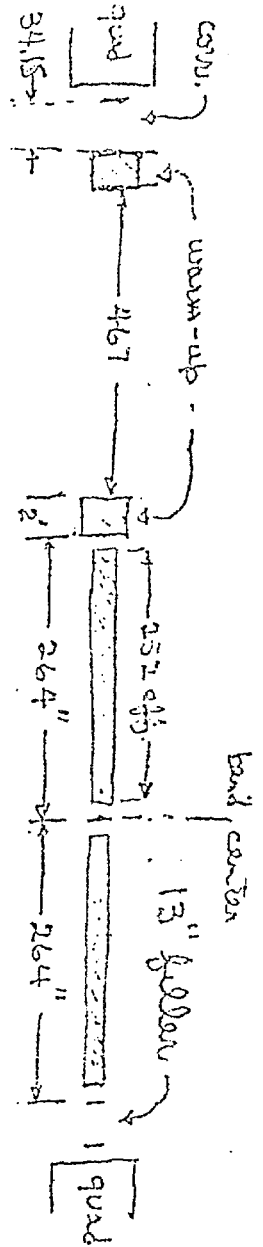
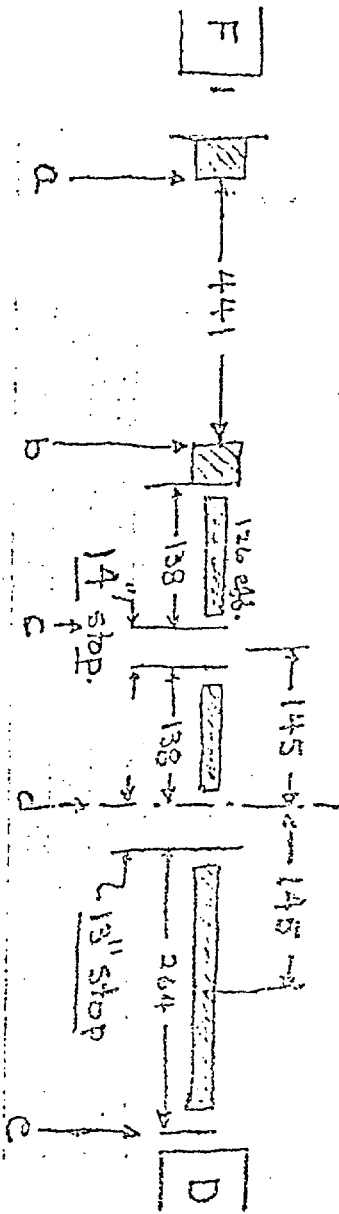


Figure 14.



Medium straight section as designed.



Medium straight - modified with 2 half-bends and using filler space to create spaces for absorbers.

Figure 15.

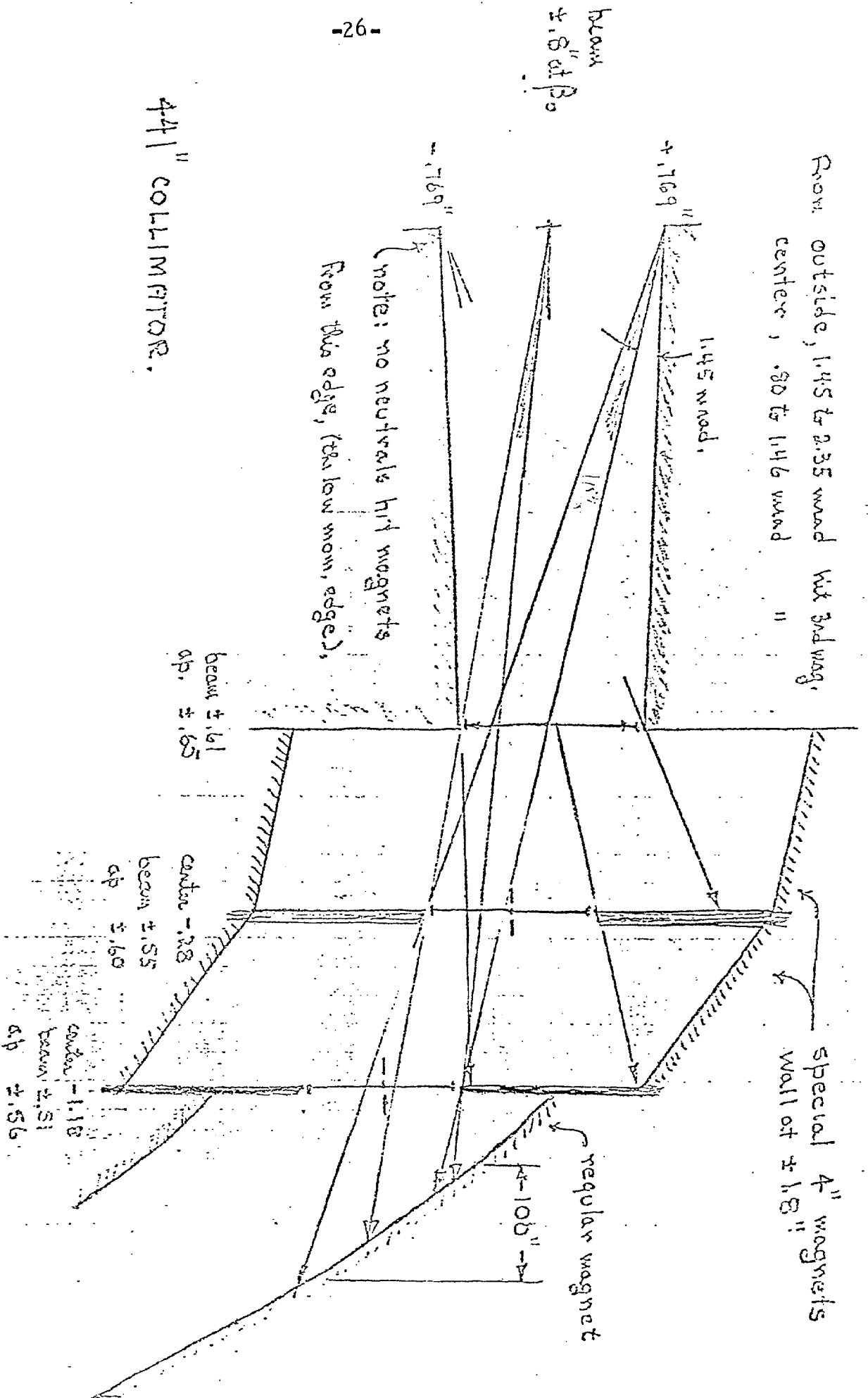


Figure 16.